Fault Diagnosis of Bearing Damage by Means of the Linear Discriminant Analysis of Stator Current Features From the Frequency Selection

Christelle Piantsop Mbo'o and Kay Hameyer

***Abstract*—Bearing damage is the most common failure in electrical machines. It can be detected by vibration analysis. However, this diagnosis method is costly or not always accessible due to the location of the equipment and the choice of the implemented sensors. An alternative method is provided with the electrical monitoring using the stator current of the electrical machine. This study aims at developing a diagnostic system based on the current feature generated by a frequency selection in the stator current spectrum. The features are evaluated by means of the linear discriminant analysis and the fault diagnosis is performed with the Bayes classifier. The proposed method is evaluated by two types of damages at different load cases. The results show that the damaged bearings can be distinguished from the healthy bearing depending on the considered load cases.**

***Index Terms*—Bayes classifier, bearing damage, fault diagnosis, linear discriminant analysis (LDA), permanent magnet synchronous motor (PMSMs), spectral analysis, stator current.**

I. Introduction

ELECTRICAL machines consist of several components, which are amongst others, stator, rotor windings, magnets in permanent magnet synchronous machines (PMSMs), shaft, or bearings. All these components may be damaged due to abrasion, overloading, unbalanced load, or electrical stress because of the control with an inverter. Machine failures can be classified into four groups: 1) bearing damages; 2) damages related to the stator; 3) the rotor; and 4) other damages [1]. Bearing damages are the most common fault [2]. The early detection of this failure is an important issue because unexpected breakdown or fatal damage of the entire drive system can be avoided. Moreover, maintenance cost can be reduced and the system reliability is increased by using the condition monitoring. Bearing damage can be detected by vibration analysis [3]–[5]. This is a reliable and standardized method for the detection of bearing damage due to fatigue failures, particularly local damages. However, the choice and the positioning of the sensors can be a challenge depending on the location of the equipment. Therefore, the diagnosis using vibration sensors is costly, not always accessible and an online monitoring cannot always be guaranteed.

An alternative method is given by the electrical monitoring by means of the stator current of the PMSM as well as the induction machine. This method uses the embedded stator current signal of the control unit, so that no additional sensors are required for the detection.

Several papers investigate the detection by means of the stator current [6]–[13]. A short overview of the results is presented here to illustrate the objective of this study. For example, Rosero *et al.* [7] discusses the detection of bearing damage within a PMSM by means of the wavelet as well as the short-time Fourier transform of a simulated nonstationary signal of the stator current. The detection using the wavelet transform gives the best results. However, the comparison between simulated and experimental results shows that the amplitude deviation of the occurred fault frequencies are very small. Picot *et al.* [8] and Obeid *et al.* [9] propose a method for the detection based on the statistical analysis of the stator current harmonics of a PMSM. The fault index bases on the frequencies multiple of the rotation frequency within the stator current spectrum. The measurements are done at specified constant speeds under no load condition. The damaged bearing can be recognized with the proposed approach, but the damage cannot be differentiated from other damages causing a change in the frequencies multiple of the rotation frequency. Silva and Cardoso [10] present a detection method of bearing damage based on the stator current of an induction machine similar as in [11]–[13]. However, the stator current is analyzed by means of the Extended Park's Vector. The considered bearing damages are holes in the outer race with three different sizes. The damage can be recognized especially for the damage with the wide diameter.

In summary, the most of the papers study artificial wide damage and the machine is loaded with the load torque only. The influence of the radial force is not considered. Moreover, the detection by means of the Fourier and Wavelet transform is commonly employed. However, it is still a challenging issue because the deviation observed between the healthy and the faulty bearing is very small. In this paper, the stator current signal is analyzed by means of the Fourier transform with the Welch's method. Instead of the observed deviation in the

Manuscript received December 3, 2015; revised March 24, 2016 and April 20, 2016; accepted May 26, 2016. Date of publication June 15, 2016; date of current version September 16, 2016. Paper 2015-EMC-1004.R2, presented at the 2015 IEEE 10th International Symposium on Diagnostics for Electrical Machines, Power Electronics, and Drives, Guarda, Portugal, Sep. 1–4, and approved for publication in the IEEE Transactions On Industry Applications by the Electric Machines Committee of the IEEE Industry Applications Society. This work was supported by the Federal Ministry of Economics and Technology (BMWi) under the Autonome Antriebstechnik durch Sensorfusion für die intelligente, simulationsbasierte Uberwachung Steuerung von Produktionsanlagen project.

The authors are with the Institute of Electrical Machines, RWTH Aachen University, Aachen 52062, Germany (e-mail: christelle.piantsop@iem.rwth-aachen.de; kay.hameyer@iem.rwth-aachen.de).

Color versions of one or more of the figures in this paper are available online at http://ieeexplore.ieee.org.

Digital Object Identifier 10.1109/TIA.2016.2581139

current spectrum, it considers a feature set of statistical values for the detection. The statistical values are calculated from the energy content of each characteristic fault frequency within a specific interval. Statistical features are combined using the linear discriminant analysis (LDA) for the fault diagnosis. The LDA is commonly used in order to obtain a maximum separation between the feature of each group. The new approach is evaluated at two type of damages in different load cases, in which the load torque, speed, and radial force are varied.

This paper is organized as follows. A short overview of the bearing damages is given in Section II, in which the bearings used for the study and their damages are presented. Section III describes the diagnosis procedure and the construction of the feature matrix. Thereby, the classification method is introduced. Section IV presents the test bench and the test procedure, while the bearing damages diagnosis by means of the proposed approach is presented in Section V. Finally, the work is summarized and concluded in Section VI.

II. Bearing Damage

Rolling bearings consist of an inner and outer race, which are separated by rolling elements such as balls or cylindrical rollers. Due to material fatigue or wearing, pitting, or flaking can occur within the bearing components. If a damage is present in the bearing, shock pulses with characteristic frequencies occur, when a ball passes through the damaged point. These characteristic frequencies depend on the affected part of the bearing and are calculated by means of the geometry of the rolling elements and the mechanical rotational frequency f_{rm}. The characteristic frequencies of each fault type are summarized in the following [14].

Outer race defect

$$f_{\text{outer}} = \frac{N_{\text{ball}}}{2} \cdot f_{\text{rm}} \cdot \left(1 - \frac{D_{\text{ball}}}{D_{\text{cage}}} \cos\beta\right). \tag{1}$$

Inner race defect

$$f_{\text{inner}} = \frac{N_{\text{ball}}}{2} \cdot f_{\text{rm}} \cdot \left(1 + \frac{D_{\text{ball}}}{D_{\text{cage}}} \cos\beta\right). \tag{2}$$

Ball defect

$$f_{\text{ball}} = f_{\text{rm}} \cdot \frac{D_{\text{cage}}}{D_{\text{ball}}} \cdot \left(1 - \frac{D_{\text{ball}}^2}{D_{\text{cage}}^2} \cos\beta^2\right). \tag{3}$$

Cage defect

$$f_{\text{cage}} = \frac{1}{2} \cdot f_{\text{rm}} \cdot \left(1 - \frac{D_{\text{ball}}}{D_{\text{cage}}} \cos\beta\right) \tag{4}$$

whereas N_{ball} is the number of balls or cylindrical rollers, β the contact angle of the balls, D_{ball} the ball or roller diameter, and D_{cage} the cage diameter, also known as the ball or roller pitch diameter.

Bearing damage causes a radial motion between the rotor and the stator, which leads to speed fluctuations resulting as oscillations in the motor current with the characteristic fault frequencies. The resulting motor current can be expressed as [15]

$$i(t) = \sum_{k=1}^{\infty} i_k \cdot \cos\left(\omega_{\text{c}_k} \cdot t + \varphi\right) \tag{5}$$

with the angular velocity ω_{c_k} and the phase angle φ. The angular velocity can be expressed as $\omega_{\text{c}_k} = \frac{2\pi \cdot f_{\text{c}_k}}{p}$, with p the pole pair number of the used machine and the frequency f_{c_k}. This frequency consists of the electric supply frequency f_{el} and the outer race fault frequency f_{outer} in the case of an outer race damage

$$\begin{aligned} f_{\text{c}_k} &= f_{\text{el}} + k \cdot f_{\text{outer}} \\ \text{with} \quad k &= \pm 1, \pm 2, \pm 3, \ldots . \end{aligned} \tag{6}$$

In the following study, cylindrical-roller bearings of type *N203E.TVP2* illustrated in Fig. 1(left), are used. This kind of bearing is selected in the investigation because of their separable components, which facilitate the creation of defects in a specific component. Three bearings are investigated in the diagnosis: one healthy and two bearings with artificial damages.[1] The damages are listed below.

1) Faulty group 1: An artificial slot in the outer race with a width of $w_1 = 0.25$ mm.
2) Faulty group 2: the outer race was wire eroded. The wire has a diameter of 8 mm, which produces a damaged point in the outer race with a width of $w_2 = 2.8$ mm, in Fig. 1 (right).

The damage size represents 0.2% and 2.6% of the raceway length, respectively.

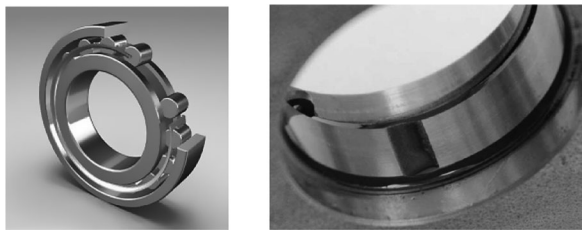

Fig. 1. Cylindrical-roller bearing (left) and bearing damage of faulty group 2 in outer race (right).

The characteristic fault frequency for the outer race fault is calculated based on the geometry of the bearing and the number of balls given in Appendix Table V. According to [1], the contact angle is 0° for cylindrical-roller bearings. Therefore, the characteristic frequency from (1) is given by

$$f_{\text{outer}} = \frac{N_{\text{ball}}}{2} \cdot f_{\text{rm}} \cdot \left(1 - \frac{D_{\text{ball}}}{D_{\text{cage}}}\right) = 4.25 \cdot f_{\text{rm}}. \tag{7}$$

III. Diagnosis Procedure

The procedure used for the fault diagnosis is illustrated in Fig. 2. The spectral density of the measured stator current is estimated using the Welch's method at first [16]. Then, frequency bands with the characteristic fault frequency as center

[1]The damage were generated at the Chair of Design and Drive Technology from the University in Paderborn, Germany.

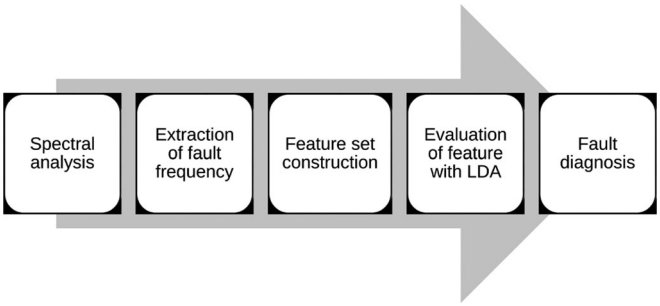

Fig. 2. Diagnosis procedure.

frequency are extracted for the construction of the feature matrix. Further steps are presented in the following.

A. Extraction of Fault Frequencies

The fault frequencies f_{c_k} of the considered bearing are calculated as explained in (6). The energy density of a specific interval, which contains a characteristic fault frequency as center frequency, is extracted. The interval limits defined in (8) depend on the frequency resolution δ in the estimated spectrum and the specified speed

$$\begin{aligned} &[f_{c_k} - B_w/2 - \delta, f_{c_k} + B_w/2] \\ &\text{with} \quad f_{c_k} = f_{el} \cdot \left(1 + k \cdot \frac{4.25}{p}\right) \\ &\text{and} \quad k = \pm 1, \pm 2, \pm 3, \ldots, \pm 10. \end{aligned} \tag{8}$$

B_w represents the minimum distance between two fault frequencies. f_{c_k} is the characteristic fault frequency in relation to the electrical frequency. This is obtained by performing the mechanical frequency in (7) as a function of the electrical frequency: $f_{rm} = \frac{f_{el}}{p}$, with p the pole pair number of the used machine. The harmonic orders of the characteristic fault frequencies are represented by $\left(1 + k \cdot \frac{4.25}{p}\right)$. The first five positive orders are 2.0625, 3.1250, 4.1875, 5.2500, 6.3125 for the studied machine, whereas the minimum distance between two fault frequencies is $B_w = 1.0625$.

As shown in [17], the first 20 characteristic frequency bands are the most significant ones for the fault diagnosis. Therefore, only these frequency bands are extracted from each stator current spectrum. The extracted frequency bands are finally reduced to 11 bands according to the following criteria.

1) Every frequency multiple of the electrical supply frequency and the specified speed is eliminated
2) Every frequency inside a frequency interval with boundaries, which includes the multiple of the electrical supply frequency is eliminated.

The eliminated frequencies can occur in the stator current spectrum with a larger amplitude than the one at the fault frequencies, so that the diagnosis results can be disturbed.

After the extraction, the feature matrix is constructed and evaluated by means of the LDA for the fault diagnosis. These will be discussed in the following.

B. Construction of the Feature Matrix

The feature matrix consists of six statistical values calculated from each extracted frequency band. The statistical features are selected based on the features, which provide good results in the fault analysis using the vibration signals [5]. These features are the standard deviation, kurtosis, skewness, crest factor, clearance, shape factor, and are given below as follows.

Standard deviation

$$x_{\text{std},k} = \sqrt{\frac{1}{l}\sum_{i=1}^{l}(y_k(i) - \bar{y}_k)^2}. \tag{9}$$

Kurtosis

$$x_{kr,k} = \frac{\frac{1}{l}\sum_{i=1}^{l}(y_k(i) - \bar{y}_k)^4}{x_{\text{std},k}^4}. \tag{10}$$

Skewness

$$x_{sk,k} = \frac{\frac{1}{l}\sum_{i=1}^{l}(y_k(i) - \bar{y}_k)^3}{x_{\text{std},k}^3}. \tag{11}$$

Crest factor

$$x_{cr,k} = \frac{\max(y_k(i))}{y_{\text{rms},k}}. \tag{12}$$

Clearance

$$x_{cl,k} = \frac{\max(y_k(i))}{y_{\text{smr},k}}. \tag{13}$$

Shape factor

$$x_{sh,k} = \frac{y_{\text{rms},k}}{\frac{1}{l}\sum_{i=1}^{l}|y_k(i)|} \tag{14}$$

with

$$\bar{y}_k = \frac{1}{l}\sum_{i=1}^{l} y_k, \quad y_{\text{smr},k} = \frac{1}{l}\sum_{i=1}^{l}\sqrt{y_k^2}$$

$$y_{\text{rms},k} = \sqrt{\frac{1}{l}\sum_{i=1}^{l} y_k^2}\ .$$

$y_k = [p_s(f_i)]$ contains the energy density of the frequencies f_i within the interval $[f_{c_k} - B_w/2 - \delta, f_{c_k} + B_w/2]$.

$\bar{y}_k$ represents the mean value, $y_{\text{rms},k}$ the root mean square value and $y_{\text{smr},k}$ the square-mean-root value. Instead of the standard deviation, the relative deviation Δ_r of the standard deviation $x_{\text{std},k}$ between the healthy and the faulty case is used as a feature

$$\begin{aligned} &\Delta_r(x_{\text{std},k}) = \frac{(|x_{std,k,\text{healthy}}| - |x_{\text{std},k,\text{faulty}}|)}{|x_{\text{std},k,\text{healthy}}|} \\ &\text{with} \quad k = \pm 1, \pm 2, \pm 3, \ldots\ . \end{aligned} \tag{15}$$

The feature matrix $\underline{X}$ contains the statistical values for each extracted frequency interval

$$\underline{X} = \begin{bmatrix} x_{\text{kr},1} & x_{\text{sk},1} & x_{\text{cr},1} & x_{\text{cl},1} & x_{\text{sh},1} & \Delta_r(x_{\text{std},1}) \\ x_{\text{kr},2} & x_{\text{sk},2} & x_{\text{cr},2} & x_{\text{cl},2} & x_{\text{sh},2} & \Delta_r(x_{\text{std},2}) \\ \ldots & \ldots & \ldots & \ldots & \ldots & \ldots \\ x_{\text{kr,k}} & x_{\text{sk,k}} & x_{\text{cr,k}} & x_{\text{cl,k}} & x_{\text{sh,k}} & \Delta_r(x_{\text{std},k}) \end{bmatrix}. \tag{16}$$

C. Evaluation of the Feature Matrix by Means of the LDA

The discriminant analysis consists of a linear combination of the feature in order to reduce the feature space and scale the feature according to its importance. Hence, a good separation between the feature set in each group can be achieved. The discriminant function calculates a discriminant value $C_i(g)$ for each observation i of the group g with the feature value x_{ij} as follows [18]:

$$\begin{aligned} C_i(g) &= b_0 + b_1 \cdot x_{i1} + b_2 \cdot x_{i2} + \cdots + b_j \cdot x_{ij} \text{ with} \\ x_{ij} &= \text{feature value } ij \quad (j = 1, \ldots 6) \text{ and } (i = 1, \ldots n), \\ b_j &= \text{discriminant coefficient for the feature } j, \\ b_0 &= \text{constant value.} \end{aligned} \tag{17}$$

The discriminant coefficients are determined by maximizing the discriminant criteria Γ,

$$\Gamma = \frac{S_b}{S_w} \tag{18}$$

which is the proportion between the between-group scatter matrix S_b and the within-group scatter matrix S_w. This optimization problem can be solved as a classical eigenvalue problem. The between-group scatter matrix evaluates the separability of different groups, while the within-class scatter matrix evaluates the compactness within each group and the between-group scatter matrix. These are defined as

$$S_\mathrm{b} = \sum_{g=1}^{G} l_g (\mu_g - \mu)(\mu_g - \mu)^T \tag{19}$$

$$S_\mathrm{w} = \sum_{g=1}^{G} \sum_{i=1}^{l_g} (x_i(g) - \mu_g)(x_i(g) - \mu_g)^T \tag{20}$$

$$\text{with } \mu_g = \frac{1}{l_g} \sum_{i=1}^{l_g} x_i(g) \text{ and } \mu = \frac{1}{l} \sum_{i=1}^{l} x_i.$$

For the fault diagnosis, the Bayes classifier is used to assign the discriminant values to each group. This is given by the posterior probability that a parameter Y_i belongs to the group g

$$\begin{aligned} P(g|Y_i) &= \frac{P(Y_i|g)P(g)}{\sum_{g=1}^{G} P(Y_i|g)P(g)} \qquad (g = 1, 2, \ldots, G) \\ &= \frac{\exp\left(-\frac{D_{ig}^2}{2}\right)P(g)}{\sum_{g=1}^{G} \exp\left(-\frac{D_{ig}^2}{2}\right)P(g)}. \end{aligned} \tag{21}$$

$P(g)$ is the prior probability of the group g and D_{ig} represent the distance between the parameter Y_i and the centroid of the group $\overline{C}(g)$. The centroid of the group is defined as the mean value of the discriminant value for each group g: $\overline{C}(g) = \frac{1}{k} \sum_{i=1}^{k} C_i(g)$. The parameters are assigned to the group with the maximum posterior probability.

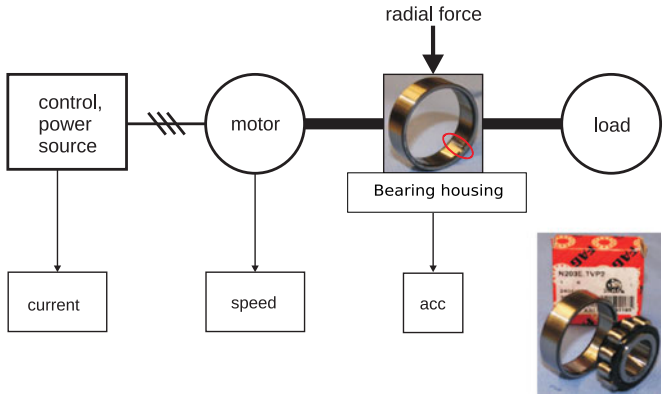

Fig. 3. Schematic setup of the test bench.

IV. Test Procedure

The test bench used for the experiments consists of a test motor, a magnetic brake (load) and a cylindrical-roller bearing in a special test-bench housing. The test motor is a 500 W vector-controlled PMSM with 4 pole pair number and a nominal torque of 1.6 Nm. The rated data of the machine are given in Table VI (Appendix B). Fig. 3 shows the schematic setup of the test bench. The bearing housing and the considered bearing damages were developed during the public research project Autonome Antriebstechnik durch Sensorfusion fur die intelligente, simulationsbasierte Uberwachung Steuerung von Produktionsanlagen[2] funded by the federal ministry of economics and technology (BMWi) [19].

The bearing housing is connected to the machine and the load through shaft couplings and is equipped with accelerometers to measure the vibration in addition. Due to the fact that a small radial load acts on the bearing of an electrical motor because of the load torque, an additional radial force is considered in this paper in order to study its influence on the bearing damage detection. Furthermore, the test motor is a drum-integrated motor for a band conveyor, which operates permanently under radial load condition. In order to apply an adjustable radial force to the bearing, a load mechanism is included in the housing of the bearing. The force is measured by a force transducer and the bearing outer race is positioned in such a way that the applied force acts exactly on the damaged area.

The currents used for the bearing fault diagnosis is measured by a current transducer, which has a measurement range up to 60 A, an accuracy of 0.05%, and a bandwidth of 5 MHz. In order to obtain a good spectral resolution, the sampling frequency for the current measurement is set to 100 kHz. The measured current is then filtered by a second-order Butterworth filter with a cutoff frequency of 12.5 kHz before recording in order to eliminate all frequencies near by the pulse frequency of the controller unit.

[2]Autonome Antriebstechnik durch Sensorfusion für die intelligente, simulationsbasierte Überwachung and Steuerung von Produktionsanlagen.

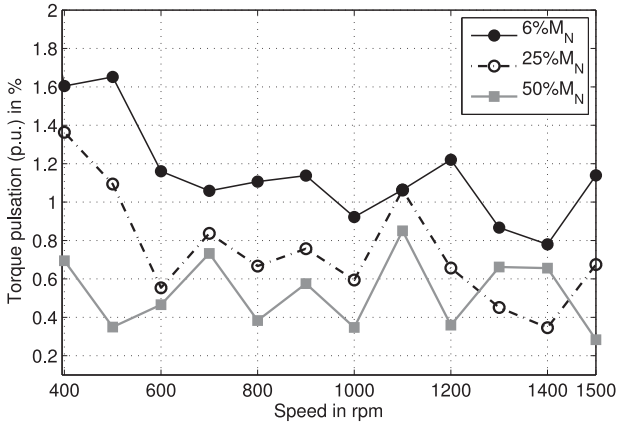

Fig. 4. Torque pulsations measured at different loads and speeds for a constant radial force of 400 N.

V. Bearing Damage Diagnosis

The proposed approach is evaluated by means of the measured stator current. The current signals are collected for the healthy and damaged bearings under different operating points. The damaged bearings are outer race faults at two different severity levels, which are presented in Section II. Two phases of the stator current are measured: 1) i_{u}; and 2) i_{v}. The motor is driven at different speeds, load torques, and radial forces.

The load cases are selected considering the results of the following analysis. The Impact of the load in the detection of bearing faults by means of the stator current was investigated in [17] for the PMSM. The results shown, that the characteristic fault frequencies due to bearing damage occur with a high amplitude at high radial load. Moreover, the raise of the loads has no significant influence on the amplitude of these frequencies.

The torque pulsation for the considered system is investigated. For this purpose, the measurements are performed at different speeds from 400 to 1500 rpm with variable load torque, which are $6\%, 25\%, 50\%$ of the nominal torque. The torque pulsations of the machine is estimated by subtraction of the set value of the load torque to the measured torque. The distribution of the estimated torque pulsations normalized by the set values, is illustrated in Fig. 4. It shows that the torque pulsations vary over the speed range and reduce with increasing loads. Its mean value over the considered speeds is 1.14% for the load of $6\%\mathrm{M_N}$. This drops to 0.75% at the load of $25\%\mathrm{M_N}$ and 0.5% at the load of $50\%\mathrm{M_N}$. Therefore, bearing damages cause torque fluctuations, which depend on the load conditions of the machine. When the torque pulsation is decreasing, the amplitude of the harmonics caused by the bearing damage also decreases. Hence, the consideration of higher load torques in this regard does not provide further advantage for the damage detection. For these reasons, the measurements are performed at a load torque of 6% of nominal torque. The values of the speed are 400 rpm 900 rpm, and 1500 rpm, while the radial force is set to 400 N, 1 kN, or 2 kN.

The measurements are then performed in the following operation points for the investigation.

1) LC1: F = 1 kN, T = 0.1 Nm, s = 900 rpm.
2) LC2: F = 2 kN, T = 0.1 Nm, s = 400 rpm.

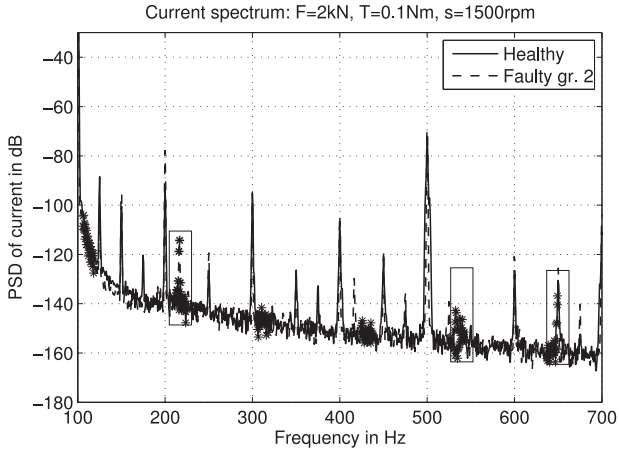

Fig. 5. Current spectrum of the healthy bearing and the bearing with the faulty group 2.

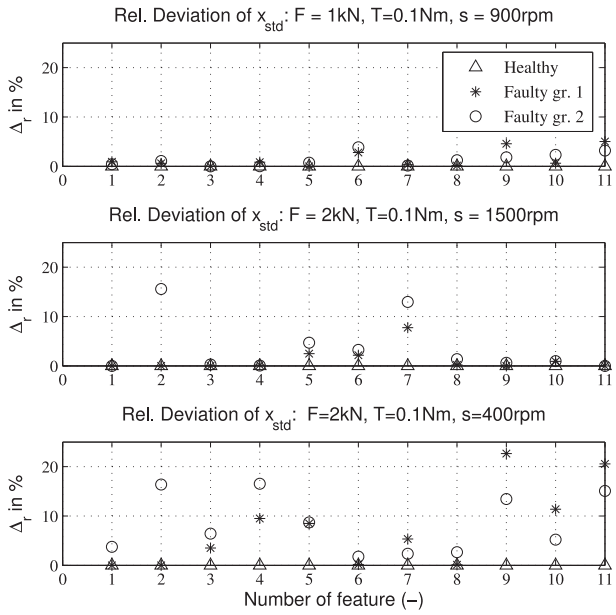

Fig. 6. Relative deviation of x_{std} for three load cases (LC1, LC2, LC3) and all groups.

3) LC3: F = 2 kN, T = 0.1 Nm, s = 1500 rpm.
4) LC4: F = 400 N, T = 0.1 Nm, s = 1500 rpm.
5) LC5: F = 400 N, T = 0.1 Nm, s = 400 rpm.

The power spectral densities of the stator current i_{u} are illustrated as an example in Fig. 5, in which two of the extracted frequency bands are marked. This current are measured in the healthy and the faulty group 2 with the load case LC3.

The measured data are spectral analyzed for two currents phases i_{u} and i_{v}. The 11 frequency bands are extracted. Then, the statistical features from (10) to (15) are calculated for the extracted frequency bands for each phase current in each group and load cases. Hence, a specific group contains a 22×6 feature matrix (16) for each load case.

Fig. 6 illustrates for example the relative deviation of x_{std} for the 11 extracted frequency intervals in the phase current i_{u} for all considered groups and three load cases. A considerable

TABLE I
CONTRIBUTION OF THE FEATURE IN THE FAULTY GROUP 1 AND IN EACH LOAD CASES

Loadcase	x_{cr}	x_{cl}	x_{kr}	x_{sh}	x_{sk}	$\Delta_r\,(x_{\mathrm{std}})$
LC1	+	o	o	-	-	-
LC2	o	o	-	-	-	+
LC3	+	o	o	-	-	-
LC4	+	o	o	-	-	-
LC5	+	o	o	-	-	o

deviation is observed at some frequencies particularly in the faulty group 2. However, the deviations at the load cases $\mathrm{F}=1\,\mathrm{kN}, \mathrm{M}=0.1\,\mathrm{Nm}$, and $\mathrm{s}=900\,\mathrm{rpm}$ are very small. The feature are evaluated in the following section.

A. Feature Evaluation

The contribution of each feature in the fault detection is evaluated for all the considered load cases. This represents the percentage of the mean value for each feature vector, which can be summarized as follows: all values greater than 25% are represented with +; values smaller than 10% are represented with $-$ and the middle values are represented with o. The contribution of the feature are summarized in Table I for the faulty group 1. This is similar to the contribution of the faulty group 2. The most significant feature in the considered load conditions is the crest factor.

The skewness and the shape factor are least important, while all the other features contribute differently depending on the load condition. Hence, the fault detection by means of a single feature is not sufficient. Therefore, the fault detection is investigated by means of the LDA, in which a linear combination of all features, named discriminant function, is used for the detection.

B. Construction of the Training Data

The used discriminant coefficients are precalculated based on a training dataset. A stochastic selection of training data for the detection is not meaningful, because the amplitude of the fault frequency and consequently the features are varied in function of the load. The training data must reflect the behavior of the system in the faulty cases. Therefore, the training data consists of the observations obtained from the measurements with the most significant characteristic harmonics. This measurement corresponds to the load case (LC2) with a total of 20% of the generated data in each group. The remaining data of the other load cases are used as test data. The discriminant function of the training data for the considered groups are illustrated in Fig. 7. The line represents the separator between the healthy and the faulty state. Only two values of the healthy state and the faulty group 2 are false assigned, while seven values of the faulty group 1 are false assigned. However, most values of the faulty bearing are located above the line. The performance of the classifier is evaluated using the confusion matrix $\underline{M}$, which is a square matrix with a size equal to the total number of values in each group. $M(i,j)$ is a count of observations known to be in group i but predicted to be in group j. The proper

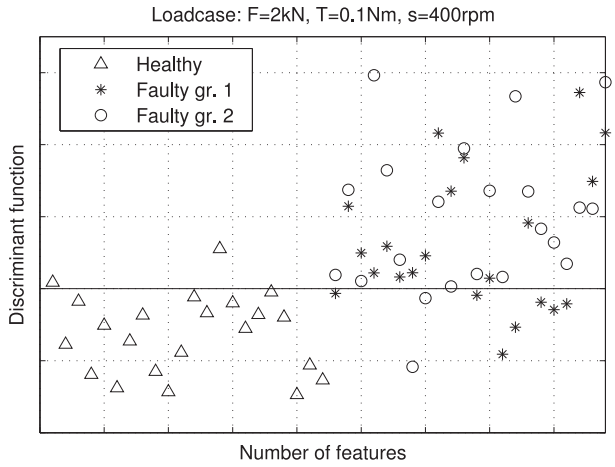

Fig. 7. Discriminant function of the training data, faulty group 1 and faulty group 2 in comparison to the healthy state at radial force 2 kN and speed $s = 400\,\mathrm{rpm}$.

TABLE II
CONFUSION MATRIX OF THE CLASSIFIER FOR THE FAULTY GROUP 1

	Healthy	Faulty	Total
Healthy	20	2	22
Faulty	7	15	22
Total	27	17	$n = 44$

predicted observations are represented with the same indices. The Accuracy of the classifier can be evaluated by means of the method proposed in [20]. This is defined as the sum of the mispredicted values over the double of the total numbers of observations n

$$\text{Accuracy} = \frac{M(i,j) + M(j,i)}{n}. \tag{22}$$

The confusion matrix of the classifier is evaluated by the healthy and faulty group 1. The result is given in Table II. The Accuracy of the classifier is considered for the faulty group 1. Seven values of the faulty group 1 are false assigned, while only two values of the healthy group are false assigned. Hence, the Accuracy is 0.2. The accuracy of the classifier is estimated with the same manner for the faulty group 2. This is 0.09. Hence, the faulty states can clearly be distinguished from the healthy ones by the training data, except at damaged with small damage size.

C. Fault Diagnosis

The fault diagnosis is performed for all measured data using the Bayes classifier (21) and the results are summarized in Tables III and IV, in which the posterior probability of the affiliation to each group is represented.

Considering the results in Table III for the bearing damage with 0.2 % damage size (faulty group 1), 64% of the values are assigned to the faulty state at the radial load F=1 kN and the specified speed s=900 rpm (LC2), while 36% are assigned to

TABLE III
POSTERIOR PROBABILITY OF THE AFFILIATION TO FAULTY GROUP 1

	Faulty group 1				
	LC1	LC2	LC3	LC4	LC5
Healthy	18 %	36 %	23 %	27 %	64 %
Faulty	82 %	64 %	77 %	73 %	36 %

TABLE IV
POSTERIOR PROBABILITY OF THE AFFILIATION TO FAULTY GROUP 2

	Faulty group 2				
	LC1	LC2	LC3	LC4	LC5
Healthy	32 %	9 %	18 %	45 %	64 %
Faulty	68 %	91 %	82 %	55 %	36 %

the healthy state. The other measurements provide better results from 73% to 82% except in the load case (LC5), in which 64% of the values are incorrectly assigned. The bearing damage cannot be distinguished in this small load condition.

The same behavior is observed at this load case LC5 in Table IV for the bearing damage with 2.6% damage size (faulty group 2). The measurements with higher radial forces or speeds (LC1, LC2, LC3) show better results, especially at the load case LC2, in which the posterior probability is 91%. Any bearing damage causes a radial motion between the rotor and the stator, which leads to a rise of the friction torque in load case. The amplitude of the characteristic frequency increases with the amplitude of the friction torque which depends on the speed and the radial load. At small radial loads and speeds, the characteristic frequencies appear with an amplitude close to the noise amplitude. Hence, a fault diagnosis is impossible at this condition. Overall, the bearing damages can be distinguished by means of the proposed approach considering the applied load cases with the exception of the small load case.

VI. SUMMARIZING AND CONCLUSION

This paper presents a new approach for the diagnosis of the bearing damage by means of the stator current signal of the PMSM. The method uses the energy content in the characteristic fault frequency in order to generate specific features for the detection. These statistical features are summarized in a feature matrix and evaluated using the LDA. For the evaluation, two bearing damages are investigated and the stator current is measured for different load cases. Thereby, the fault diagnosis is performed by means of the Bayes classifier. The bearing damage can be identified and distinguished from the healthy bearing with the proposed method under the considered load cases except in the load conditions with small speeds and radial forces. Hence, the fault diagnosis is impossible in small load conditions. However, this method provides promising results for the detection of the bearing damage using the stator current, when the training data are not stochastically selected values. These must be chosen from the load cases, which reflect the behavior of the system in faulty case at the best.

APPENDIX A
DATA OF THE USED CYLINDRICAL-ROLLER BEARING

TABLE V
DATA OF THE USED CYLINDRICAL-ROLLER BEARING

	N203E-TVP2
inner diameter d	17 mm
outer diameter D	40 mm
roller diameter D_{ball}	6.5 mm
cage diameter D_{cage}	28.6 mm
raceway groove radius r_a	17.55 mm
number of balls/rollers N_{ball}	11

APPENDIX B
DATA OF THE USED MACHINE (RATED VALUES)

TABLE VI
DATA OF THE USED MACHINE (RATED VALUES)

	PMSM
power	500 W
pole pair	4
current	2.3 A
speed	3000 rpm
torque	1.6 Nm
moment of inertia	0.4239 kgcm^2
direct inductance L_{sd}	28.6 mH
quadrature inductance L_{sq}	31.6 mH
resistance R_s at 20°C	5.6 Ω

ACKNOWLEDGMENT

The authors would like to thank the participating companies and research institutions for their cooperation.

REFERENCES

[1] P. Tavner, L. Ran, J. Penman, and H. Sedding, *Condition Monitoring of Rotating Electrical Machines*. Stevenage, U.K.: The Institution of Engineering and Technology, 2008.

[2] P. O'Donnell and IEEE Motor Reliability Working Group, "Report of large motor reliability survey of industrial and commercial installations, part I," *IEEE Trans. Ind. Appl.*, vol. IA-21, no. 4, pp. 853–864, Jul. 1985.

[3] W. Zhou, B. Lu, T. Habetler, and R. Harley, "Incipient bearing fault detection via motor stator current noise cancellation using wiener filter," *IEEE Trans. Ind. Appl.*, vol. 45, no. 4, pp. 1309–1317, Jul./Aug. 2009.

[4] M. Delgado, G. Cirrincione, A. Garcia, J. Ortega, and H. Henao, "A novel condition monitoring scheme for bearing faults based on curvilinear component analysis and hierarchical neural networks," in *Proc. XXth Int. Conf. Elect. Mach.*, 2012, pp. 2472–2478.

[5] X. Jin, M. Zhao, T. Chow, and M. Pecht, "Motor bearing fault diagnosis using trace ratio linear discriminant analysis," *IEEE Trans. Ind. Electron.*, vol. 61, no. 5, pp. 2441–2451, May 2014.

[6] R. Schoen, B. Lin, T. Habetler, J. Schlag, and S. Farag, "An unsupervised, on-line system for induction motor fault detection using stator current monitoring," *IEEE Trans. Ind. Appl.*, vol. 31, no. 6, pp. 1280–1286, Nov. 1995.

[7] J. Rosero, L. Romeral, E. Rosero, and J. Urresty, "Fault detection in dynamic conditions by means of discrete wavelet decomposition for pmsm running under bearing damage," in *Proc. 24th Annu. IEEE Appl. Power Electron. Conf. Expo.*, 2009, pp. 951–956.

[8] A. Picot, Z. Obeid, J. Regnier, P. Maussion, S. Poignant, and O. Darnis, "Bearing fault detection in synchronous machine based on the statistical analysis of stator current," in *Proc. 38th Annu. Conf. IEEE Ind. Electron. Soc.*, Oct. 2012, pp. 3862–3867.

[9] Z. Obeid, S. Poignant, J. Regnier, and P. Maussion, "Stator current based indicators for bearing fault detection in synchronous machine by statistical frequency selection," in *Proc. 37th Annu. Conf. IEEE Ind. Electron. Soc.*, 2011, pp. 2036–2041.

[10] J. Silva and A. J. M. Cardoso, "Bearing failures diagnosis in three-phase induction motors by extended park's vector approach," in *31st Annu. Conf. IEEE Ind. Electron. Soc.*, 2005, pp. 2591–2596.

[11] R. Obaid, T. Habetler, and J. Stack, "Stator current analysis for bearing damage detection in induction motors," in *Proc. 4th IEEE Int. Symp. Diag. Elect. Mach., Power Electron. Drives*, 2003, pp. 182–187.

[12] F. Immovilli, M. Cocconcelli, A. Bellini, and R. Rubini, "Detection of generalized-roughness bearing fault by spectral-kurtosis energy of vibration or current signals," *IEEE Trans. Ind. Electron.*, vol. 56, no. 11, pp. 4710–4717, Nov. 2009.

[13] A. Soualhi, G. Clerc, H. Razik, and A. Lebaroud, "Fault detection and diagnosis of induction motors based on hidden Markov model," in *Proc. XXth Int. Conf. Elect. Mach.*, 2012, pp. 1693–1699.

[14] J. Stack, T. Habetler, and R. Harley, "Fault classification and fault signature production for rolling element bearings in electric machines," in *Proc. 4th IEEE Int. Symp. Diag. Elect. Mach. Power Electron. Drives*, 2003, pp. 172–176.

[15] M. Blodt, P. Granjon, B. Raison, and G. Rostaing, "Models for bearing damage detection in induction motors using stator current monitoring," *IEEE Trans. Ind. Electron.*, vol. 55, no. 4, pp. 1813–1822, Apr. 2008.

[16] P. Welch, "The use of fast fourier transform for the estimation of power spectra: A method based on time averaging over short, modified periodograms," *IEEE Trans. Audio Electroacoustics*, vol. 15, no. 2, pp. 70–73, Jun. 1967.

[17] C. Piantsop Mbo'o, T. Herold, and K. Hameyer, "Impact of the load in the detection of bearing faults by using the stator current in PMSMs," in *Proc. Int. Conf. Elect. Mach.*, Sep. 2014, pp. 1621–1627.

[18] S. Mika, G. Ratsch, J. Weston, B. Scholkopf, and K. Muller, "Fisher discriminant analysis with kernels," in *Proc. IEEE Signal Process. Society Workshop Neural Netw. Signal Process. IX*, Aug. 1999, pp. 41–48.

[19] C. Lessmeier, C. Piantsop Mbo'o, I. Coenen, D. Zimmer, and K. Hameyer, "Untersuchung von Bauteilschäden elektrischer Antriebsstränge im Belastungsprhüfstand mittels Statorstromanalyse," *ANT J. Technische Fachzeitschriften der Vereinigten Fachverlage GmbH*, vol. 1, pp. 8–13, 2012.

[20] I. Martin-Diaz, O. Duque-Perez, R. Romero-Troncoso, and D. Morinigo-Sotelo, "Supervised diagnosis of induction motor faults: A proposed methodology for an improved performance evaluation," in *Proc. IEEE 10th Int. Symp. Diag. Elect. Mach. Power Electron. Drives*, Sep. 2015, pp. 359–365.

Kay Hameyer (M'96–SM'99) received the M.Sc. degree in electrical engineering from the University of Hannover, Hannover, Germany, and the Ph.D. degree from the Berlin University of Technology, Berlin, Germany.

After his university studies, he worked at Robert Bosch GmbH, Stuttgart, Germany, as a Design Engineer for permanent magnet servo motors and vehicle board net components. Until 2004, he was a Full Professor for Numerical Field Computations and Electrical Machines at KU Leuven, Belgium. Since 2004, he has been a Full Professor and the Director of the Institute of Electrical Machines, RWTH Aachen University, Germany. His research interests include numerical field computation and optimization, and the design and controls of electrical machines. He is author of more than 250 journal publications, more than 500 international conference publications, and four books.

Dr. Hameyer is a member of Verband der Elektrotechnik, Elektronik, und Informationstechnik, and a fellow of the Institution of Engineering and Technology.

Christelle Piantsop Mbo'o was born in 1982 in Douala, Cameroon. She received the Dipl.-Ing. degree in electrical engineering from RWTH Aachen University, Aachen, Germany, in 2008.

Since 2009, she has been a Researcher with the Institute of Electrical Machines, RWTH Aachen University. Her research interests include analysis and design of electrical machines.